Atmos. Chem. Phys. Discuss., 13, 11659–11688, 2013
www.atmos-chem-phys-discuss.net/13/11659/2013/
doi:10.5194/acpd-13-11659-2013

Atmospheric Chemistry and Physics Discussions
Open Access

CO profiles from SCIAMACHY observations using cloud slicing and comparison with model simulations

C. Liu[1,*], S. Beirle[1], T. Butler[1,], P. Hoor[1,***], C. Frankenberg[2], P. Jöckel[1,****], M. Penning de Vries[1], U. Platt[3], A. Pozzer[1,4], M. G. Lawrence[1,**], J. Lelieveld[1,4], H. Tost[1,***], and T. Wagner[1]**

[1]Max-Planck-Institute for Chemistry, Mainz, Germany
[2]Jet Propulsion Laboratory, California Institute of Technology, Pasadena, USA
[3]Institute for Environmental Physics, University of Heidelberg, Germany
[4]Cyprus Institute, Nicosia, Cyprus
[*]now at: Harvard-Smithsonian Center for Astrophysics, Cambridge, MA, USA
[**]now at: Institute for Advanced Sustainability Studies e.V., Potsdam, Germany
[***]now at: Institute for Atmospheric Physics, University Mainz, Germany
[****]now at: Institut für Physik der Atmosphäre, Deutsches Zentrum für Luft- und Raumfahrt (DLR), Oberpfaffenhofen, Germany

Received: 11 April 2013 – Accepted: 25 April 2013 – Published: 2 May 2013

Correspondence to: T. Wagner (thomas.wagner@mpic.de)

Published by Copernicus Publications on behalf of the European Geosciences Union.

ACPD
13, 11659–11688, 2013

Abstract

We apply a cloud slicing technique (CST), originally developed for Total Ozone Mapping Spectrometer (TOMS) ozone observations, to CO vertical column densities retrieved from the SCanning Imaging Absorption spectroMeter for Atmospheric CHartographY (SCIAMACHY). CST makes use of the shielding effect of clouds and combines trace gas column measurements of cloudy pixels with different cloud heights to retrieve fractional columns aloft. Here we determine seasonal mean tropospheric CO profiles at a vertical resolution of 1 km, which is much finer than what can be obtained from thermal IR instruments. However, since both the atmospheric CO profiles and the effective cloud heights depend systematically on meteorology, the profiles retrieved from the CST have to be interpreted with care. We compare the seasonal mean SCIAMACHY CO profiles with the output from two atmospheric models sampled in the same way as the satellite observations. We find systematic differences both in the absolute values and vertical and horizontal gradients. The results indicate that vertical (re)distributions of emissions and their strengths are not well represented in the models. It seems likely that deep convective transport is underestimated.

1 Introduction

Carbon monoxide (CO) is emitted into the atmosphere by natural and anthropogenic processes. It is toxic in high concentrations and is an important precursor of tropospheric ozone (e.g. Crutzen and Gidel, 1983). The atmospheric lifetime of CO is typically weeks to months (Cicerone, 1988), thus it is an ideal tracer for atmospheric transport processes (Logan et al., 1981; Lelieveld et al., 2001; Shindell et al., 2006).

It has been shown in several studies, including satellite observations (e.g., Gloudemans et al., 2006, 2009; de Laat et al., 2006, 2007, 2010; Kopacz et al., 2010 ; Liu et al., 2011), that current CO emission inventories tend to underestimate source strengths, especially in regions with strong anthropogenic pollution. These findings are confirmed

ACPD
13, 11659–11688, 2013

in this study. Beyond this, here we derive CO concentration profiles, from which information on atmospheric transport patterns can be derived.

We analyse observations of SCIAMACHY on board the ENVISAT satellite (Burrows et al., 1995; Bovensmann et al., 1999). Our retrieval of the total atmospheric CO vertical column density (VCD) and its validation is described in detail in Liu et al. (2011).

Following up on the work of Liu et al. (2011) here we focus on cloud covered pixels with effective cloud fractions > 10 %. This allows us to apply the so-called cloud slicing technique (CST) (Ziemke et al., 1998, 2001; Ziemke and Chandra, 1999), based on the assumption that clouds shield absorption by the atmosphere below the cloud top. Because of the rather low surface albedo, this assumption is mostly fulfilled for observations in the near IR spectral range, even for observations with relatively small cloud fractions.

Information on effective cloud height and cloud fraction for individual SCIAMACHY CO observations is taken from the FRESCO$^+$ algorithm (Fast REtrieval Scheme for Cloud from the Oxygen A band, see Koelemeijer et al. (2001), and Wang et al., 2008) derived from the same SCIAMACHY observations.

Because of the relatively large uncertainties of the individual SCIAMACHY CO measurements (typically several tens of percent, see Frankenberg et al., 2005b; de Laat et al., 2006; Liu et al., 2011) and the relatively low sampling frequency (global coverage after 6 days), averages over rather long periods have to be calculated to achieve meaningful height profiles. In this study seasonal averages over three years (2003–2005) are presented. Our CO profiles have a relatively fine vertical resolution of 1 km, much higher than can be obtained from satellite observations in the thermal IR (see e.g., Drummond and Mand, 1996; Deeter et al., 2003; Rinsland et al., 2006; George et al., 2009; Worden et al., 2010, 2013; McMillan et al., 2011). It should, however, be noted that the retrieved profiles do not represent true atmospheric profiles, but complex composites, which combine measurements made under different meteorological conditions. Thus their direct interpretation is difficult and a detailed quantitative interpretation is only possible by comparison with atmospheric models, from which the output

ACPD
13, 11659–11688, 2013

is processed according to the same principle. In this study seasonal means of the SCIAMACHY CO profiles are compared to two models: MATCH (Model of Atmospheric Transport and Chemistry, von Kuhlmann et al., 2003) and EMAC (ECHAM5/MESSy Atmospheric Chemistry modelling system, Jöckel et al., 2006). The seasonal means are based on model data sampled at the exact locations and times of the individual SCIAMACHY observations.

The paper is organised as follows: in Sect. 2, we introduce the satellite retrieval and the CST. In Sect. 3 we present and discuss selected comparison results between satellite observations and models. Section 4 provides our conclusions.

2 Retrieval of atmospheric CO profile information from SCIAMACHY

We use SCIAMACHY CO columns derived using the Iterative maximum a posteriori (IMAP)-DOAS method (Frankenberg et al., 2005a,b); the CO VCDs were normalised using MOPITT observations over the ocean as described in Liu et al. (2011). However, different from the study of Liu et al. (2011), here we use only observations for (partly) cloudy conditions (effective cloud fractions > 10 %). We combine the CO columns with effective cloud fraction and effective cloud height from the FRESCO$^+$ algorithm (Koelemeijer et al., 2001; Wang et al., 2008) (see also Sect. 2.1).

In the near-infrared fitting range for CO (2324 nm to 2335 nm), the wavelength is sufficiently long that Rayleigh scattering can be neglected. Therefore, the photons that the satellite detects are either scattered by the cloud or reflected at the Earth's surface. Although within the spectral range of the CO analysis clouds are not as bright as in the visible spectral range (see e.g., Nakajima and King, 1990), the signal from the clouded part usually still dominates the measured spectra, which thus mainly contains information from the atmospheric above the cloud.

We apply the CST in the following way: in a first step, the observed CO VCDs are averaged for selected (intervals of) effective cloud heights. Here it should be noted that the effective cloud height from the FRESCO$^+$ algorithm systematically underestimates

ACPD
13, 11659–11688, 2013

the geometric cloud top height (see Sect. 2.1). Thus here we use the term "effective cloud height". In this study we use intervals of 1 km from the surface to 9 km:

$$\mathrm{PVCD}_{z_m^*} = \frac{\sum_{z_m<z_i<z_{m+1}} \mathrm{VCD}_{z_i}}{N} \quad (1)$$

Here z_m and z_{m+1} are the lower and upper boundary of a selected height interval and z_m^* is the average cloud height of all observations with cloud heights within that interval. In this study z_m^* is typically within $z_m + 0.4$ km and $z_m + 0.6$ km. N is the number of all observations used in Eq. (1).

PVCD represents the average partial CO VCD above the respective average effective cloud heights. Global maps of seasonally averaged PVCDs for different cloud heights are presented in Fig. 1. Note that in addition to the clear sky total CO VCD (Liu et al., 2011), the CO PVCDs retrieved for cloudy satellite pixels cover also the oceans. Especially for low cloud heights, strong spatial gradients are found with the highest values over regions with strong CO emission sources. Also a strong inter-hemispheric gradient is found. Note that gaps are present especially over deserts because we removed all observations over surfaces with an albedo > 40 %. Over highly reflective surfaces cloud algorithms are known to have increased uncertainties. In the maps for low cloud heights gaps are also found over regions with high mountains.

With increasing cloud height, less measurements are available leading to larger scatter or even gaps in the maps of the CO PVCDs. But, as expected the CO PVCDs systematically decrease with altitude. In contrast to the systematic dependence of the CO PVCD on cloud height, the CO PVCDs are almost independent of the selected effective cloud fraction threshold (see Fig. 2).

From successive pairs of CO PVCDs it is in principle possible to derive the average CO concentration in the layer between both cloud top altitudes:

$$[\mathrm{CO}]_{z_m^{**}} = \frac{\mathrm{PVCD}_{z_m^*} - \mathrm{PVCD}_{z_{m+1}^*}}{z_m^* - z_{m+1}^*} \quad (2)$$

ACPD
13, 11659–11688, 2013

with z^{**}_m the average of z^{*}_m and z^{*}_{m+1}.

However, in contrast to the original application of the CST, here we do not determine and discuss such average CO concentration profiles, but focus on profiles of CO PVCDs because of three reasons:

a. Despite the fact that large amounts of individual observations are averaged, in some cases the PVCDs are not a smooth function of altitude. This is either caused by "atmospheric noise", or random errors of the measurements. In such cases, concentration profiles as derived from Eq. (2) would show unrealistic oscillations.

b. Since most of the CO sources are located close to the surface, and the sinks are distributed over a large range of the atmosphere, CO concentrations (and also PVCDs) are expected to decrease systematically with altitude. Such behaviour is indeed found for most cases. Nevertheless, in some regions, especially in cases of effective convection over strong emission sources, increasing CO PVCDs are found at high altitudes. Note, that in these regions partial columns from CST for different cloud tops are not related to the same atmospheric state (i.e. CO profile). Thus, they represent CO profiles occurring during different times with differing cloud conditions and thus CO partial columns. For such observations, the application of Eq. (2) would lead to unphysical negative CO concentrations.

c. Systematic offsets of the CO PVCDs cancel out when applying Eq. (2). Thus information about the absolute values of the CO PVCDs would be lost.

We calculated seasonal averages using measurements over 3 yr (2003–2005). For the comparison with the model data, SCIAMACHY observations are gridded on the model resolution (T42, corresponding to a Gaussian grid of approximately 2.8° × 2.8°).

In order to use as many observations as possible we chose a rather low threshold for the effective cloud fraction of 10 %. The good agreement of CO PVCDs for different lower thresholds (Fig. 2) indicates an effective shielding effect even for small cloud fractions. Part of the good agreement is probably also caused by the fact that the averages are dominated by observations made at larger cloud fractions.

ACPD
13, 11659–11688, 2013

Finally, it should again be emphasised that although large numbers of observations were averaged, the atmospheric profiles retrieved by the CST are not per se representative of the true average atmospheric profiles, since cloud type (and cloud altitude) are systematically correlated to meteorology and atmospheric transport patterns (e.g. convective updraft) and chemistry. The retrieved profile information has thus to be interpreted with care. A meaningful quantitative interpretation is only possible by comparison with atmospheric model simulations sampled in the same way as the satellite observations, see Sect. 3.

It should also be noted that the CO PVCDs might be affected by spectral interference with the much stronger absorptions of H_2O and CH_4. And, since the absorptions of H_2O and CH_4 systematically depend on cloud altitude, the CO PVCDs might be subject to a systematic bias varying with cloud altitude. Nevertheless, such potential spectral interference can not explain the localised enhancements of the CO PVCDs over strong emission sources (see Sects. 3.3 and 3.4).

2.1 Interpretation of the effective cloud height

The FRESCO$^+$ algorithm used for the determination of the effective cloud height describes clouds as so called Lambertian reflectors (with an assumed albedo of 80 %) (Koelemeijer et al., 2001). Nevertheless, a significant fraction of the solar photons detected by the satellite instrument may have penetrated into the cloud. Thus they may have encountered stronger O_2 absorption than assumed by the Lambertian cloud model and the effective cloud height retrieved by the FRESCO$^+$ algorithm would systematically underestimate the true (geometric) cloud top height: on average the FRESCO$^+$ cloud height rather represents the middle of the cloud layer than the cloud top (Wang et al., 2008; Sneep et al., 2008). Also at the wavelength used for the CO analysis (2330 nm), a fraction of the detected solar photons has penetrated into the cloud leading to systematically higher CO PVCDs than that for the geometric cloud top height. Compared to the FRESCO$^+$ algorithm (at 760 nm), the effect is, however,

ACPD
13, 11659–11688, 2013

smaller than for the spectral range used for the CO analysis (2330 nm), because of the stronger absorption by the cloud droplets.

Both effects (underestimation of the cloud top height and overestimation of the CO PVCDs) complicate the quantitative comparison between satellite observations and model results, and without detailed information on cloud properties and CO concentration profiles it is not possible to correct the associated uncertainties. Fortunately, they have only minor influence on the main findings of our study because in general the (relative) atmospheric CO concentration profile decreases with altitude, following similar lapse rates as the oxygen concentration. Thus the underestimation of the cloud top height and the overestimation of the CO PVCDs to a large extent compensate. In other words: The retrieved (too low) cloud top height fits well to the retrieved (too high) CO PVCD.

It should also be noted that the main conclusions of our study are related to the comparison of spatial patterns rather than absolute values of the CO PVCDs. While especially above high clouds the absolute values of the CO PVCDs probably overestimate the true values, the spatial patterns, especially in horizontal dimension, are only slightly affected.

Figure 2 shows a comparison of CO PVCDs retrieved for different lower thresholds of the effective cloud fraction. The very good agreement indicates that the systematic biases introduced by the penetration of solar photons into the cloud layers have probably only a small effect on the profiles of CO PVCDs.

3 Comparison to atmospheric models

In this section, we compare CO profiles from SCIAMACHY observations with the results of two atmospheric models (MATCH-MPIC and EMAC). One important aspect of the comparison is that only coincident data are compared: model outputs are sampled at the times and locations of the SCIAMACHY observations. CO PVCDs are calculated from the simulated concentration profiles above the effective cloud height determined

ACPD
13, 11659–11688, 2013

by the FRESCO$^+$ algorithm. We applied this procedure, because of the rather coarse resolution of the model data. However, since the cloud information is only taken from the SCIAMACHY measurements and not from the models, situations of different meteorological conditions might be compared, potentially introducing systematic biases between the satellite and model data.

To estimate the magnitude of these potential biases, we also calculated mean model profiles without any cloud filtering for the same seasons (see Sect. 3.3). We found that these average profiles are very similar to those using the data selection criterion based on SCIAMACHY cloud data, indicating that the latter are well representative for the average CO concentration profiles. The good agreement between both data sets is related to the rather long atmospheric lifetime of CO and the averaging over large areas and long periods.

Both models are using the same input emissions (for details see below). However, a major difference between the two models is that MATCH-MPIC is a Chemistry Transport Model (CTM), driven by NCEP data, while EMAC is an Atmospheric Chemistry General Circulation model (AC-GCM), which for the simulation analysed here was nudged towards ECMWF operational analysis data.

3.1 MATCH-MPIC

MATCH-MPIC (Model of Atmospheric Transport and CHemistry – Max Planck Institute for Chemistry version) is a global, three dimensional chemical transport model representing tropospheric O_3, CH_4, NO_x, and VOC chemistry. MATCH-MPIC has been described and evaluated in detail (Rasch et al., 1997; Lawrence et al., 1999, 2003; von Kuhlmann et al., 2003). MATCH-MPIC is run in a semi-offline mode, relying only on a limited set of input fields (surface pressure, geo potential, temperature, horizontal winds, surface latent and sensible heat fluxes, and zonal and meridional wind stresses). These fields are obtained from the NCEP GFS (National Centers for Environmental Prediction Global Forecast System, Kalnay et al., 1990). Fields are interpolated in time to the model time step of 30 min, and used to diagnose online the transport by

ACPD
13, 11659–11688, 2013

advection, vertical diffusion and deep convection, as well as the tropospheric hydrological cycle (water vapour transport, cloud condensate formation and precipitation). The model uses a combination of two convection parameterisations which focus on deep and shallow mixing (Zhang and McFarlane, 1995; Hack, 1994). Anthropogenic emissions are from the Emissions Database for Atmospheric Research (EDGAR) fast track 2000 emissions, which are based on the EDGAR 3.2 emissions inventory (Olivier and Berdowski, 2001). Biomass burning emission data are based on the Global Fire Emissions Database (GFED v2), van der Werf et al. (2006).

3.2 EMAC

The ECHAM/MESSy Atmospheric Chemistry (EMAC) model is a numerical chemistry and climate simulation system that includes sub-models describing tropospheric and middle atmosphere processes and their interaction with oceans, land and human influences (Jöckel et al., 2010). It uses the Modular Earth Sub-model System (MESSy, version 2.3; Jöckel et al., 2005) to link multi-institutional computer codes. The core atmospheric model is the 5th generation European Centre Hamburg general circulation model (ECHAM version 5.3.02, Röckner et al., 2006). For the present study we applied EMAC in the T42L90MA-resolution, i.e. with a spherical truncation of T42 (corresponding to a quadratic Gaussian grid of approx. 2.8 by 2.8 degrees in latitude and longitude) with 90 vertical hybrid pressure levels up to 0.01 hPa (middle atmosphere). Like in MATCH-MPIC, in the EMAC set-up the biomass burning emissions are taken from the Global Fire Emission Database (GFED v2) (van der Werf et al., 2006), and the anthropogenic emissions from the EDGAR3.2FT2000.

Model output for analysis was triggered every 5 h of simulation time. For EMAC, the prognostic variables vorticity, divergence, temperature and the (logarithm of the) surface pressure have been nudged to the operational ECMWF analysis data in order to allow a point-to-point comparison to the satellite data (see Jöckel et al., 2010). Primary emissions and dry deposition of trace gases and aerosols were calculated with the submodels ONLEM, OFFLEM, TNUDGE (Kerkweg et al., 2006a), and DRYDEP (Kerkweg

ACPD
13, 11659–11688, 2013

et al., 2006b), respectively. EMAC parameterizes convection following Tiedtke (1989) and Nordeng (1994) for both deep and shallow convection. More details on the overall model set-up (including emissions) are presented by Jöckel et al. (2006 and 2010) and Pozzer et al. (2007).

3.3 Comparison of height profiles for selected regions

In this section we quantitatively compare the measured CO profiles (PVCDs) for different regions (see Fig. 3). The selected regions either represent clean oceanic regions remote from strong emission sources or areas with strong CO emissions caused e.g. by biomass burning or anthropogenic activities related to industry, traffic and energy use. Figure 4 presents seasonally averaged profiles of the CO PVCDs derived from SCIAMACHY observations and the MATCH and EMAC models. Note that in addition to the average model profiles (using the SCIAMACHY cloud selection criterion, see Sect. 2) also average EMAC CO profiles based on all model profiles without cloud slicing are shown (dark green). The fact that good agreement is found between the model profiles obtained using SCIAMACHY cloud selection on the one hand, and model profiles constructed without cloud selection on the other hand, indicates that profiles using SCIAMACHY cloud selection are representative of average conditions.

The columns in Fig. 4 show data for January–March, April–June, July–September, and October–December. The last two rows show results for the remote ocean (regions 9 and 10 in Fig. 3). In general, the SCIAMACHY derived PVCDs are higher, particularly in the Northern Hemisphere. The reason for these differences is not completely clear, but similar latitudinally dependent differences between satellite observations (SCIAMACHY and MOPITT) and model results were also reported in other studies (e.g. Gloudemans et al., 2009, De Laat et al., 2010). Also Liu et al. (2011) found larger differences between SCIAMACHY and models in the Northern Hemisphere (for mainly cloud-free observations over land surfaces). Interestingly, the differences between the SCIAMACHY profiles and those from MATCH and EMAC stay rather constant between

ACPD
13, 11659–11688, 2013

0.5 km and 8.5 km (except over the northern ocean in July–September and the southern ocean in October–December).

The first four rows in Fig. 4 present profile comparisons over polluted continental regions. Over China (region 8 in Fig. 3), the satellite profiles show systematically larger values than the models, in agreement with other studies (e.g. Liu et al., 2011 and references therein). In addition the vertical gradients found with SCIAMACHY are different from those found in both models: While at the highest altitudes the model values are very similar to those over the remote oceans, at the surface they are 3 to 4 times higher. The vertical gradients in the upper troposphere in the SCIAMACHY profiles are systematically smaller than in the models, indicating that vertical transport from the polluted boundary layer is probably systematically underestimated in the models. Of course, horizontal transport from other polluted regions could also play a role, but by investigating latitudinal/longitudinal-height cross sections (Sect. 3.4), we find no evidence for this hypothesis. We do not expect the vertical distribution of anthropogenic CO emissions to be an important factor because sensitivity tests have shown that this has a small influence on CO in the free troposphere (Pozzer et al., 2009). However, this may be different for biomass burning emissions.

In other regions, which are seasonally polluted by biomass burning (6, 7, 9, three upper rows in Fig. 4), the SCIAMACHY PVCDs are also systematically larger than the model profiles during the biomass burning seasons. In some cases the gradients of the SCIAMACHY profiles are again smaller than those of the models, but this effect is less pronounced than over China. Here it should be noted that the areas of the selected biomass burning regions are rather large (much larger than the selected area over China). Thus the profiles over biomass burning regions represent averages over different height profiles in the different parts of the selected regions.

Interestingly, for the seasons without biomass burning, the differences between SCIAMACHY observations and the models are usually smaller than over the remote ocean, despite the fact that the vertical gradients are much stronger than over the remote ocean.

ACPD
13, 11659–11688, 2013

Additional comparisons of CO profiles from SCIAMACHY observations and model simulations (for regions 2, 5, 6, and 7) are presented in the Supplement.

3.4 Comparison of latitude/longitude-height cross sections

In this section we compare latitudinal-height and longitudinal-height cross sections of CO PVCDs derived from SCIAMACHY observations and models. Such comparisons allow the study of the horizontal variation of the CO profiles and can thus yield information about the processes causing the differences between measured and simulated CO profiles.

Zonal and meridional cross sections are calculated from CO PVCDs over latitude/longitude intervals of 20° (7 zonal cross sections from 80° N to 60° S, 18 meridional cross sections from 180° W to 180° E) for each season. Thus in total, 100 cross sections are calculated, which are all presented in the Supplement. In general, very good agreement between SCIAMACHY observations and model results is found (except for the systematic underestimation of the measurements by the models discussed above), with some distinct differences discussed below.

In the following, we show 7 selected cross sections (Figs. 5–7) representing cases with interesting differences between SCIAMACHY observations and models. It should be noted that the colour scales are different for SCIAMACHY observations and models to account for the systematic differences of both data sets (shifted by 5×10^{17} molec cm^{-2}).

The first example (Fig. 5) shows meridional and zonal cross sections for January to March over China. Also presented in Fig. 5 is the global map of the total (cloud free) CO VCD for the same season (from Liu et al., 2011). A strong increase of the CO columns is found over China, both in the SCIAMACHY observations and model results. However, the CO PVCDs at high altitudes in the SCIAMACHY data are systematically higher compared to the models over China (similar to Fig. 4). One important finding from Fig. 5 is that these enhanced CO PVCDs columns are clearly related to the surface emissions from China rather than to horizontal transport from other sources,

ACPD
13, 11659–11688, 2013

because the enhanced values at high altitude appear at the same longitude and latitude of the strong enhancements of the surface concentration. Thus this comparison indicates that vertical transport is probably systematically underestimated in the models. Considering the discrepancies throughout the troposphere, e.g. also at the surface in polluted regions, it seems likely that additionally the source strengths in the emission inventories are also underestimated.

Figure 6 shows cross sections for January to March over biomass burning regions in Africa. As for the cross sections above China, the CO PVCDs from the SCIAMACHY observations are systematically larger than the model data in the upper troposphere. However, in this example, the SCIAMACHY data not only indicate effective upward transport, but also a tilt of the biomass burning "plume" in the meridional cross section. In (northern) winter the plume is inclined towards the north, because the inner tropical convergence zone (ITCZ) is located south of the biomass burning region. The effective upward transport and the tilt of the biomass burning "plumes" is not seen in the model results.

Similar results are also found in cross sections for July to September in biomass burning regions in Africa and South America (Fig. 7). Similar as in Fig. 6, the SCIAMACHY observations show higher values than the models in the upper troposphere. In addition, slanting the biomass burning plumes are seen over both regions (a tilt towards the south is found which corresponds to a northerly location of the ITCZ in this season). Interestingly a tilt is not only found in the meridional cross sections, but also in the zonal cross section. These spatial patterns are not found in the model data, which might be related to the vertical distribution of biomass burning emissions in the model, partly related to mixing processes between the boundary layer and the free troposphere. It should be noted that both models show better agreement in Fig. 7 than in Fig. 6.

These findings indicate that vertical transport might not be well described in the models in some cases. Especially for emissions in the Tropics this seems to have important consequences, because of the strong impact on the inter-hemispheric distribution of trace gases.

ACPD
13, 11659–11688, 2013

Although different parameterisation schemes for convection are used in both models, the respective trigger criteria are relatively similar and the strength of the convective cloud base mass flux is in both cases determined from the available convective available potential energy. However, even though the schemes are theoretically relatively similar, a comparison in EMAC (Tost et al., 2006) showed substantial differences. Future studies investigating in detail the effects of the different parameterizations should be performed to better understand the differences between (SCIAMACHY) observations and model simulations.

4 Conclusions

We apply the cloud slicing technique (CST) to CO vertical column densities retrieved from the Scanning Imaging Absorption spectrometer for Atmospheric CHartographY (SCIAMACHY) for 2003–2005. Our CO profiles range from 0.5 km to 9.5 km and have a vertical resolution of 1 km, which is much higher compared to other satellite CO data sets, e.g. retrieved in the thermal IR. However, with the CST it is not possible to retrieve CO profiles for individual observations, but instead large data sets have to be averaged (here we use seasonal averages for the years 2003–2005). Also, since both the atmospheric CO profiles and the effective cloud heights depend systematically on meteorology, the retrieved average CO profiles do not represent exact profiles and have to be interpreted with care. For the same reason, we determine profiles of the partial CO column densities instead of the CO concentrations: in some cases the partial CO column densities for higher cloud altitudes are larger than for lower cloud altitudes which would cause negative CO concentrations if simple differences are formed.

We compare the SCIAMACHY CO profiles with two atmospheric models (MATCH-MPIC and EMAC) sampled in the same way as the satellite observations. In general we find good agreement of the spatial patterns between measurements and model results (except over regions with strong CO emission sources).

ACPD
13, 11659–11688, 2013

Systematic differences are found for the absolute values, for which we have no clear explanation. Such differences were, however, also found in earlier studies (e.g., Gloudemans et al., 2006; de Laat et al., 2006, 2007, 2010; Gloudemans et al., 2009; Kopacz et al., 2010 ; Liu et al., 2011), and are probably related to uncertainties of the used emission inventories in addition to uncertainties of the CO measurements. But the different spatial patterns are unlikely to be caused by such error sources.

We investigated the systematic differences in the spatial patterns for several regions: over China, at high altitudes, systematically higher values are found in the SCIAMACHY observations compared to the models. These differences indicate that vertical distributions of emissions, i.e. plume lofting and convective transport processes are probably underestimated by the models (see e.g. Tost et al., 2010).

Over biomass burning regions in Africa and South America, the biomass burning plumes observed by SCIAMACHY typically reach much higher altitudes than those in the model data. In addition, they are tilted according to the relative location of the ITCZ. Again, these findings indicate that the vertical distributions of emissions and/or vertical transport might not be well described in the models for these cases. Especially for emissions in the Tropics this can have important consequences, because of the strong impact on the inter-hemispheric distribution of trace gases (not only CO).

Similar studies using the CST for satellite observations of CO might also be performed for other sensors, e.g., for the near-IR and thermal IR channels from MOPITT, or other nadir-looking IR instruments like TES or IASI. The CO CST will particularly be interesting for the upcoming SENTINEL missions. The SCIAMACHY CO profiles can be made available on request.

Supplementary material related to this article is available online at: http://www.atmos-chem-phys-discuss.net/13/11659/2013/acpd-13-11659-2013-supplement.pdf.

ACPD
13, 11659–11688, 2013

Acknowledgements. We like to thank the European Space Agency (ESA) operation center in Frascati (Italy) for making the SCIAMACHY spectral data available. FRESCO$^+$ cloud data were obtained from Tropospheric Emission Monitoring Internet Service, http://www.temis.nl/fresco/. This work was supported by the National Natural Science Funds of China (Grant No. 41105011).

The service charges for this open access publication
have been covered by the Max Planck Society.

References

Bovensmann, H., Burrows, J. P., Buchwitz, M., Frerick, J., Noel, S., Rozanov, V. V., Chance, K. V., and Goede, A. P. H.: SCIAMACHY: Mission objectives and measurement modes, J. Atmos. Sci., 56, 127–150, 1999.

Burrows, J. P., Hoelzle, E., Goede, A. P. H., Visser, H., and Fricke, W.: Sciamachy – scanning imaging absorption spectrometer for atmospheric chartography, Acta Astronaut., 35, 445–451, 1995.

Cicerone, R. J.: How has the Atmospheric Concentration of CO changed, in: The Changing Atmosphere, edited by: Rowland, F. S. and Isaksen, I. S. A., Wiley, 1988.

Crutzen, P. J. and Gidel, L. T.: A two-dimensional photochemical model of the atmosphere. 2: The tropospheric budgets of anthropogenic chlorocarbons CO, CH_4, CH_3Cl and the effect of various. NO_x sources on tropospheric ozone. J. Geophys. Res., 88, 6641–6661, 1983.

Deeter, M. N., Emmons, L. K., Francis, G. L., Edwards, D. P., Gille, J. C., Warner, J. X., Khattatov, B., Ziskin, D., Lamarque, J. F., Ho, S. P., Yudin, V., Attie, J. L., Packman, D., Chen, J., Mao, D., and Drummond, J. R.: Operational carbon monoxide retrieval algorithm and selected results for the MOPITT instrument, J. Geophys. Res.-Atmos., 108, 4399, doi:10.1029/2002jd003186, 2003.

de Laat, A. T. J., Gloudemans, A. M. S., Schrijver, H., van den Broek, M. M. P., Meirink, J. F., Aben, I., and Krol, M.: Quantitative analysis of SCIAMACHY carbon monoxide total column measurements, Geophys. Res. Lett., 33, L07807, doi:10.1029/2005gl025530, 2006.

de Laat, A. T. J., Gloudemans, A. M. S., Aben, I., Krol, M., Meirink, J. F., van der Werf, G. R., and Schrijver, H.: Scanning imaging absorption spectrometer for atmospheric chartography car-

ACPD
13, 11659–11688, 2013

bon monoxide total columns: statistical evaluation and comparison with chemistry transport model results, J. Geophys. Res.-Atmos., 112, D21306, doi:10.1029/2007jd009378, 2007.
de Laat, A. T. J., Gloudemans, A. M. S., Aben, I., and Schrijver, H.: Global evaluation of SCIAMACHY and MOPITT carbon monoxide column differences for 2004–2005, J. Geophys. Res.-Atmos., 115, D06307, doi:10.1029/2009jd012698, 2010.
Drummond, J. R. and Mand, G. S.: The measurements of pollution in the troposphere (MOPITT) instrument: overall performance and calibration requirements, J. Atmos. Ocean. Tech., 13, 314–320, 1996.
Frankenberg, C., Platt, U., and Wagner, T.: Iterative maximum a posteriori (IMAP)-DOAS for retrieval of strongly absorbing trace gases: Model studies for CH_4 and CO_2 retrieval from near infrared spectra of SCIAMACHY onboard ENVISAT, Atmos. Chem. Phys., 5, 9–22, doi:10.5194/acp-5-9-2005, 2005a.
Frankenberg, C., Platt, U., and Wagner, T.: Retrieval of CO from SCIAMACHY onboard ENVISAT: detection of strongly polluted areas and seasonal patterns in global CO abundances, Atmos. Chem. Phys., 5, 1639–1644, doi:10.5194/acp-5-1639-2005, 2005b.
George, M., Clerbaux, C., Hurtmans, D., Turquety, S., Coheur, P.-F., Pommier, M., Hadji-Lazaro, J., Edwards, D. P., Worden, H., Luo, M., Rinsland, C., and McMillan, W.: Carbon monoxide distributions from the IASI/METOP mission: evaluation with other space-borne remote sensors, Atmos. Chem. Phys., 9, 8317–8330, doi:10.5194/acp-9-8317-2009, 2009.
Gloudemans, A. M. S., Krol, M. C., Meirink, J. F., de Laat, A. T. J., van der Werf, G. R., Schrijver, H., van den Broek, M. M. P., and Aben, I.: Evidence for long-range transport of carbon monoxide in the Southern Hemisphere from SCIAMACHY observations, Geophys. Res. Lett., 33, L16807, doi:10.1029/2006gl026804, 2006.
Gloudemans, A. M. S., de Laat, A. T. J., Schrijver, H., Aben, I., Meirink, J. F., and van der Werf, G. R.: SCIAMACHY CO over land and oceans: 2003–2007 interannual variability, Atmos. Chem. Phys., 9, 3799–3813, doi:10.5194/acp-9-3799-2009, 2009.
Hack, J. J.: Parameterization of moist convection in the national center for atmospheric research community climate model (CCM2), J. Geophys. Res., 99, 5551–5568, 1994.
Jöckel, P., Sander, R., Kerkweg, A., Tost, H., and Lelieveld, J.: Technical Note: The Modular Earth Submodel System (MESSy) – a new approach towards Earth System Modeling, Atmos. Chem. Phys., 5, 433–444, doi:10.5194/acp-5-433-2005, 2005.
Jöckel, P., Tost, H., Pozzer, A., Brühl, C., Buchholz, J., Ganzeveld, L., Hoor, P., Kerkweg, A., Lawrence, M. G., Sander, R., Steil, B., Stiller, G., Tanarhte, M., Taraborrelli, D.,

ACPD
13, 11659–11688, 2013

van Aardenne, J., and Lelieveld, J.: The atmospheric chemistry general circulation model ECHAM5/MESSy1: consistent simulation of ozone from the surface to the mesosphere, Atmos. Chem. Phys., 6, 5067–5104, doi:10.5194/acp-6-5067-2006, 2006.

Jöckel, P., Kerkweg, A., Pozzer, A., Sander, R., Tost, H., Riede, H., Baumgaertner, A., Gromov, S. and Kern, B.: Development Cycle 2 of the Modular Earth Submodel System (MESSy2), Geosci. Model Dev. Discuss., 3, 1423–1501, 2010.

Kalnay, E., Kanamitsu, M., and Baker, W. E.: Global numerical weather prediction at the national-meteorological-center, B. Am. Meteorol. Soc., 71, 1410–1428, 1990.

Kerkweg, A., Sander, R., Tost, H., and Jöckel, P.: Technical note: Implementation of prescribed (OFFLEM), calculated (ONLEM), and pseudo-emissions (TNUDGE) of chemical species in the Modular Earth Submodel System (MESSy), Atmos. Chem. Phys., 6, 3603–3609, doi:10.5194/acp-6-3603-2006, 2006a.

Kerkweg, A., Buchholz, J., Ganzeveld, L., Pozzer, A., Tost, H., and Jöckel, P.: Technical Note: An implementation of the dry removal processes DRY DEPosition and SEDImentation in the Modular Earth Submodel System (MESSy), Atmos. Chem. Phys., 6, 4617–4632, doi:10.5194/acp-6-4617-2006, 2006b.

Koelemeijer, R. B. A., Stammes, P., Hovenier, J. W., and de Haan, J. F.: A fast method for retrieval of cloud parameters using oxygen a band measurements from the global ozone monitoring experiment, J. Geophys. Res., 106, 3475–3490, 2001.

Kopacz, M., Jacob, D. J., Fisher, J. A., Logan, J. A., Zhang, L., Megretskaia, I. A., Yantosca, R. M., Singh, K., Henze, D. K., Burrows, J. P., Buchwitz, M., Khlystova, I., McMillan, W. W., Gille, J. C., Edwards, D. P., Eldering, A., Thouret, V., and Nedelec, P.: Global estimates of CO sources with high resolution by adjoint inversion of multiple satellite datasets (MOPITT, AIRS, SCIAMACHY, TES), Atmos. Chem. Phys., 10, 855–876, 2010, http://www.atmos-chem-phys.net/10/855/2010/.

Lawrence, M. G., Crutzen, P. J., Rasch, P. J., Eaton, B. E., and Mahowald, N. M.: A model for studies of tropospheric photochemistry: description, global distributions, and evaluation, J. Geophys. Res.-Atmos., 104, 26245–26277, 1999.

Lawrence, M. G., Rasch, P. J., von Kuhlmann, R., Williams, J., Fischer, H., de Reus, M., Lelieveld, J., Crutzen, P. J., Schultz, M., Stier, P., Huntrieser, H., Heland, J., Stohl, A., Forster, C., Elbern, H., Jakobs, H., and Dickerson, R. R.: Global chemical weather forecasts for field campaign planning: predictions and observations of large-scale features during MI-

ACPD
13, 11659–11688, 2013

NOS, CONTRACE, and INDOEX, Atmos. Chem. Phys., 3, 267–289, doi:10.5194/acp-3-267-2003, 2003.

Lelieveld, J., Crutzen, P. J., Andreae, M. O., Brenninkmeijer, C. A. M., Campos, T., Cass, G. R., Dickerson, R. R., Fischer, H., de Gouw, J. A., Hansel, A., Jefferson, A., Kley, D., de Laat, A. T. J., Lal, S., Lawrence, M. G., Lobert, J. M., Mayol-Bracero, O., Mitra, A. P. Novakov, T., Oltmans, S. J., Prather, K. A., Ramanathan, V., Reiner, T., Rodhe, H., Scheeren, H. A., Sikka D., and Williams, J.: The Indian Ocean experiment: widespread air pollution from South and South–East Asia, Science 291, 1031–1036, 2001.

Liu, C., Beirle, S., Butler, T., Liu, J., Hoor, P., Jöckel, P., Penning de Vries, M., Pozzer, A., Frankenberg, C., Lawrence, M. G., Lelieveld, J., Platt, U., and Wagner, T.: Application of SCIAMACHY and MOPITT CO total column measurements to evaluate model results over biomass burning regions and Eastern China, Atmos. Chem. Phys., 11, 6083–6114, doi:10.5194/acp-11-6083-2011, 2011.

Logan, J. A., Prather, M. J., Wofsy, S. C., and Mcelroy, M. B.: Tropospheric chemistry – a global perspective, J. Geophys. Res.-Oc. Atm., 86, 7210–7254, 1981.

McMillan, W. W., Evans, K. D., Barnet, C. D., Maddy, E. S., Sachse, G. W., and Diskin, G. S.: Validating the AIRS Version 5 CO Retrieval With DACOM In Situ Measurements During INTEX-A and -B, IEEE T. Geosci. Remote, 49, 2802–2813, doi:10.1109/TGRS.2011.2106505, 2011.

Nakajima, T. and King, M. D.: Determination of the optical-thickness and effective particle radius of clouds from reflected solar-radiation measurements, 1. Theory, J. Atmos. Sci., 47, 1878–1893, 1990.

Nordeng, T. E.: Extended versions of the convective parametrization scheme at ECMWF and their impact on the mean and transient activity of the model in the Tropics, Tech. Rep., 2006, ECWMF, 1994.

Olivier, J. G. J. and Berdowski, J. J. M.: Global emissions sources and sinks. In: The Climate System, edited by Berdowski, J., Guicherit, R. and Heij, B. J., A. A. Balkema Publishers/Swets and Zeitlinger Publishers, Lisse, the Netherlands, 33–78, 2001.

Pozzer, A., Jöckel, P., Tost, H., Sander, R., Ganzeveld, L., Kerkweg, A., and Lelieveld, J.: Simulating organic species with the global atmospheric chemistry general circulation model ECHAM5/MESSy1: a comparison of model results with observations, Atmos. Chem. Phys., 7, 2527–2550, doi:10.5194/acp-7-2527-2007, 2007.

ACPD
13, 11659–11688, 2013

Pozzer, A., Jöckel, P., and Van Aardenne, J.: The influence of the vertical distribution of emissions on tropospheric chemistry, Atmos. Chem. Phys., 9, 9417–9432, doi:10.5194/acp-9-9417-2009, 2009.

Rasch, P. J., Mahowald, N. M., and Eaton, B. E.: Representations of transport, convection, and the hydrologic cycle in chemical transport models: Implications for the modeling of short-lived and soluble species, J. Geophys. Res.-Atmos., 102, 28127–28138, 1997.

Rinsland, C. P., Luo, M., Logan, J. A., Beer, R., Worden, H. M., Kulawik, S. S., Rider, D., Osterman, G., Gunson, M., Eldering, A., Goldman, A., Shephard, M. W., Clough, S. A., Rodgers, C., Lampel, M. C., and Chiou, L.: Nadir measurements of carbon monoxide distributions by the tropospheric emission spectrometer instrument onboard the aura spacecraft: overview of analysis approach and examples of initial results, Geophys. Res. Lett., 33, L22806, doi:10.1029/2006GL027000, 2006.

Roeckner, E., Brokopf, R., Esch, M., Giorgetta, M., Hagemann, S., Kornblueh, L., Manzini, E., Schlese, R., Schulzweida, U.: Sensitivity of simulated climate to horizontal and vertical resolution in the ECHAM5 atmosphere model, J. Climate, 19, 3771–3791, 2006.

Shindell, D. T., Faluvegi, G., Stevenson, D. S., Krol, M. C., Emmons, L. K., Lamarque, J. F., Petron, G., Dentener, F. J., Ellingsen, K., Schultz, M. G., Wild, O., Amann, M., Atherton, C. S., Bergmann, D. J., Bey, I., Butler, T., Cofala, J., Collins, W. J., Derwent, R. G., Doherty, R. M., Drevet, J., Eskes, H. J., Fiore, A. M., Gauss, M., Hauglustaine, D. A., Horowitz, L. W., Isaksen, I. S. A., Lawrence, M. G., Montanaro, V., Muller, J. F., Sneep, M., de Haan, J. F., Stammes, P., Wang, P., Vanbauce, C., Joiner, J., Vasilkov, A. P., and Levelt, P. F.: Three-way comparison between OMI and PARASOL cloud pressure products, J. Geophys. Res., 113, D15S23, doi:10.1029/2007JD008694, 2008.

Pitari, G., Prather, M. J., Pyle, J. A., Rast, S., Rodriguez, J. M., Sanderson, M. G., Savage, N. H., Strahan, S. E., Sudo, K., Szopa, S., Unger, N., van Noije, T. P. C., and Zeng, G.: Multimodel simulations of carbon monoxide: comparison with observations and projected near-future changes, J. Geophys. Res.-Atmos., 111, D19306, doi:10.1029/2006jd007100, 2006.

Tiedtke, M.: A comprehensive mass flux scheme for cumulus parameterization in large-scale models, Mon. Wea. Rev., 117, 1779–1800, 1989.

Tost, H., Jöckel, P., and Lelieveld, J.: Influence of different convection parameterisations in a GCM, Atmos. Chem. Phys., 6, 5475–5493, doi:10.5194/acp-6-5475-2006, 2006.

Tost, H., Lawrence, M. G., Brühl, C., Jöckel, P., The GABRIEL Team, and The SCOUT-O3-DARWIN/ACTIVE Team: Uncertainties in atmospheric chemistry modelling due to convec-

ACPD
13, 11659–11688, 2013

tion parameterisations and subsequent scavenging, Atmos. Chem. Phys., 10, 1931–1951, doi:10.5194/acp-10-1931-2010, 2010.
van der Werf, G. R., Randerson, J. T., Giglio, L., Collatz, G. J., Kasibhatla, P. S., and Arellano Jr., A. F.: Interannual variability in global biomass burning emissions from 1997 to 2004, Atmos. Chem. Phys., 6, 3423–3441, doi:10.5194/acp-6-3423-2006, 2006.
von Kuhlmann, R., Lawrence, M. G., Crutzen, P. J., and Rasch, P. J.: A model for studies of tropospheric ozone and nonmethane hydrocarbons: model description and ozone results, J. Geophys. Res.-Atmos., 108, 4294, doi:10.1029/2002jd002893, 2003.
Wang, P., Stammes, P., van der A, R., Pinardi, G., and van Roozendael, M.: FRESCO$^+$: an improved O_2 A-band cloud retrieval algorithm for tropospheric trace gas retrievals, Atmos. Chem. Phys., 8, 6565–6576, doi:10.5194/acp-8-6565-2008, 2008.
Worden, H. M., Deeter, M. N., Edwards, D. P., Gille, J. C., Drummond, J. R., and Nédélec, P.: Observations of near-surface carbon monoxide from space using MOPITT multispectral retrievals, J. Geophys. Res., 115, D18314, doi:10.1029/2010JD014242, 2010.
Worden, H. M., Deeter, M. N., Frankenberg, C., George, M., Nichitiu, F., Worden, J., Aben, I., Bowman, K. W., Clerbaux, C., Coheur, P. F., de Laat, A. T. J., Detweiler, R., Drummond, J. R., Edwards, D. P., Gille, J. C., Hurtmans, D., Luo, M., Martínez-Alonso, S., Massie, S., Pfister, G., and Warner, J. X.: Decadal record of satellite carbon monoxide observations, Atmos. Chem. Phys., 13, 837–850, doi:10.5194/acp-13-837-2013, 2013.
Zhang, G. J. and McFarlane, N. A.: Sensitivity of climate simulations to the parameterization of cumulus convection in the Canadian climate centre general circulation model, Atmos.-Ocean, 33, 407–446, 1995.
Ziemke, J. R. and Chandra, S.: Seasonal and interannual variabilities in tropical tropospheric ozone, J. Geophys. Res., 104, 21425–21442, doi:10.1029/1999JD900277, 1999.
Ziemke, J. R., Chandra, S., and Bhartia, P. K.: Two new methods for deriving tropospheric column ozone from TOMS measurements: the assimilate UARS MLS/HALOE and convective-cloud differential techniques, J. Geophys. Res., 103, 22115–22127, 1998.
Ziemke, J. R., Chandra, S., and Bhartia, P. K.: "Cloud slicing": a new technique to derive upper tropospheric ozone from satellite measurements, J. Geophys. Res., 106, 9853–9867, doi:10.1029/2000JD900768, 2001.

ACPD
13, 11659–11688, 2013

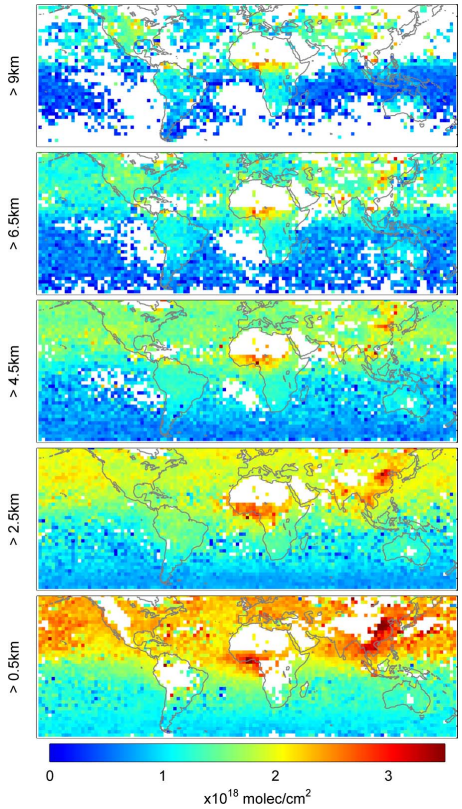

Fig. 1. CO PVCDs for different cloud heights derived from SCIAMACHY measurements from January to March of 2003–2005. Gaps are caused by missing measurements or low number of measurements, e.g. over desert regions and high mountains.

ACPD
13, 11659–11688, 2013

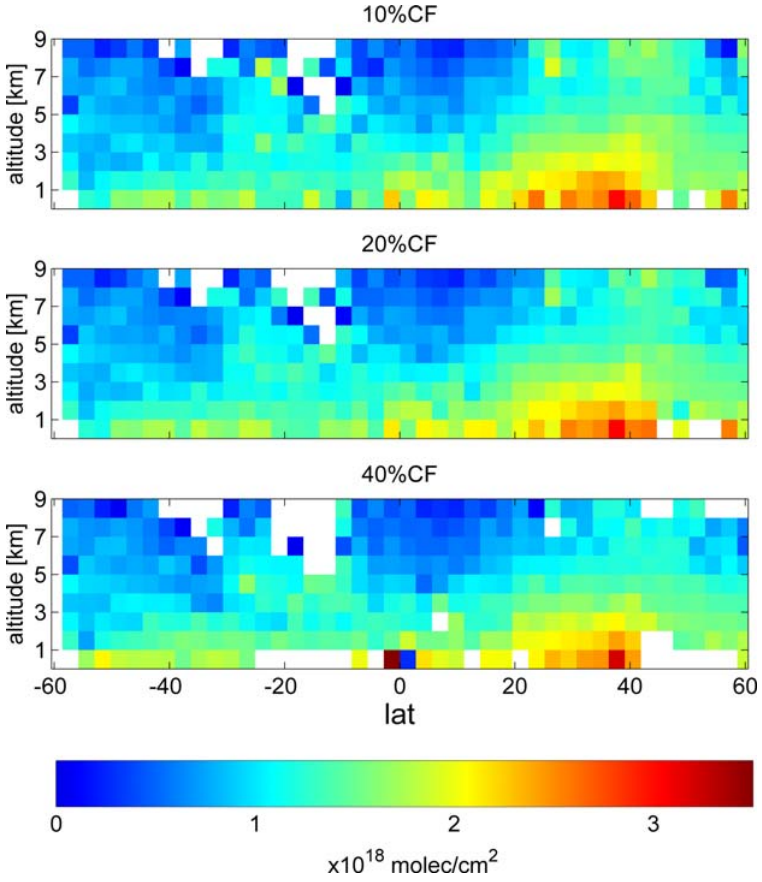

Fig. 2. Example of a meridional cross section of CO PVCDs (averaged over 100° to 120° E for July–September 2003–2005). The spatial patterns and also the absolute values of the PVCDs for the different thresholds of the effective cloud fraction are almost identical. Using more strict selection criteria, for some locations, no measurements are available for certain cloud altitudes.

ACPD
13, 11659–11688, 2013

CO profiles from SCIAMACHY cloud slicing

C. Liu et al.

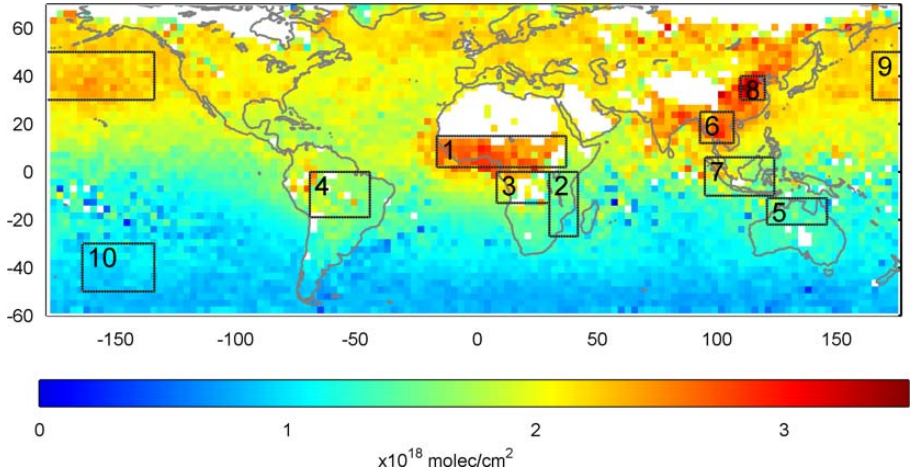

Fig. 3. Mean CO PVCDs (units: molec cm^2) retrieved from SCIAMACHY (January to March 2003–2005) for cloud fractions > 10 % and 1 km < cloud height < 2 km. The boxes indicate regions that are selected for quantitative comparison between SCIAMACHY observations and model simulations.

ACPD
13, 11659–11688, 2013

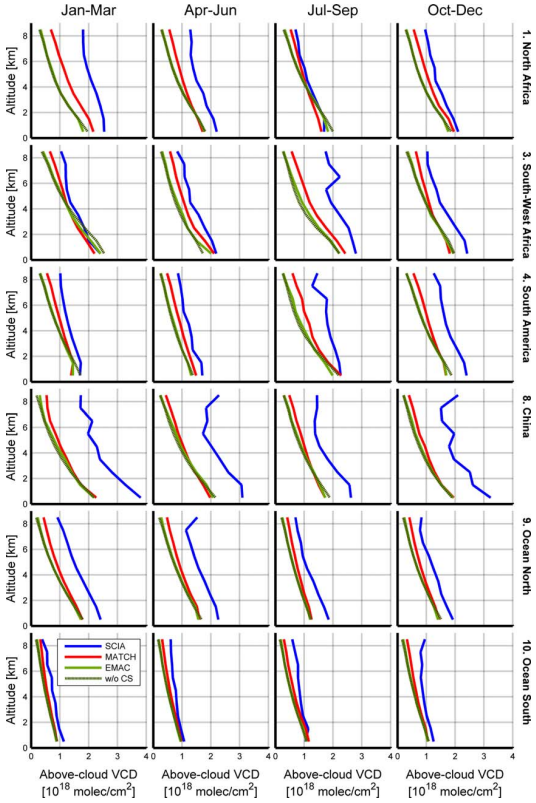

Fig. 4. Comparison of seasonally averaged profiles of CO PVCDs from SCIAMACHY observations and model simulations for selected regions (see Fig. 3). The dark green lines indicate EMAC results without cloud slicing (see text).

ACPD
13, 11659–11688, 2013

CO profiles from SCIAMACHY cloud slicing

C. Liu et al.

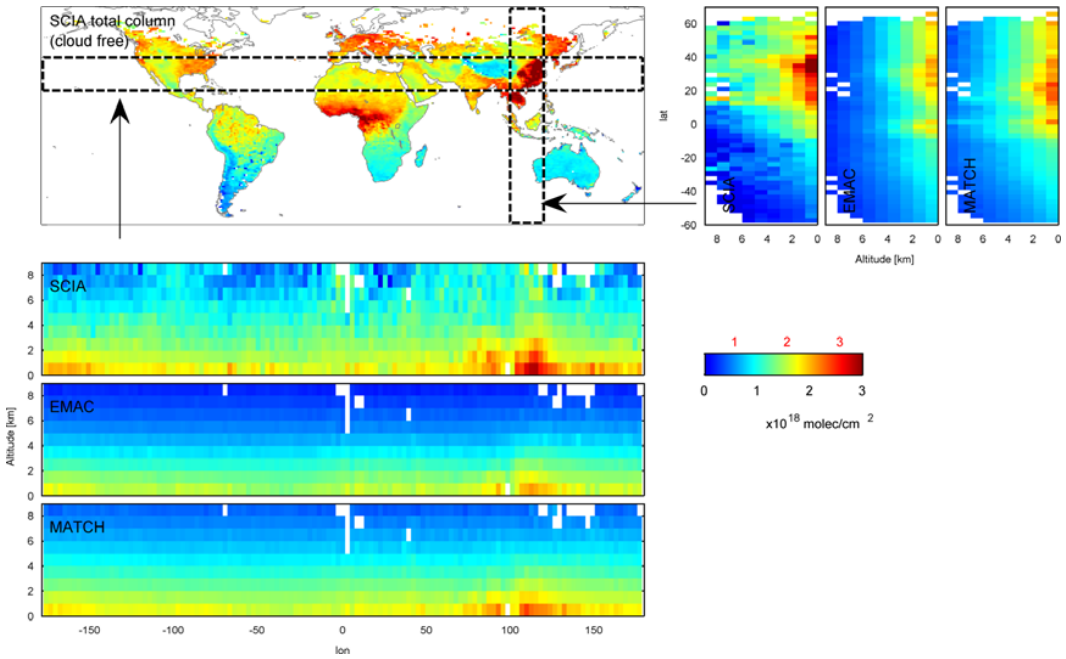

Fig. 5. Top left: global distribution of the total CO VCD for January–March derived from mainly clear sky SCIAMACHY observations (Liu et al., 2011). Top right: meridional cross sections of profiles of CO PVCDs for the same season derived from SCIAMACHY observations and model simulations. Bottom: zonal cross sections of profiles of CO PVCDs for the same season derived from SCIAMACHY observations and model simulations. Note that the colour scale is different for satellite observations and models (SCIAMACHY: red numbers on top of colour bar; models: black numbers below colour bar).

ACPD
13, 11659–11688, 2013

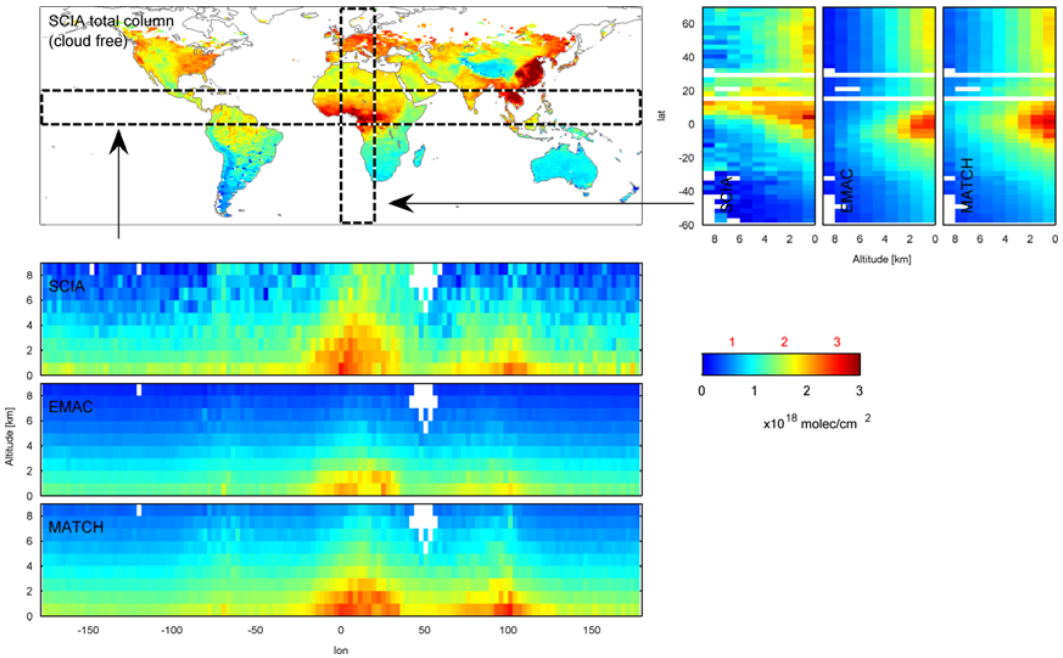

Fig. 6. Same as Fig. 5, but for meridional and zonal cross sections (January–March) over Africa.

ACPD
13, 11659–11688, 2013

CO profiles from SCIAMACHY cloud slicing

C. Liu et al.

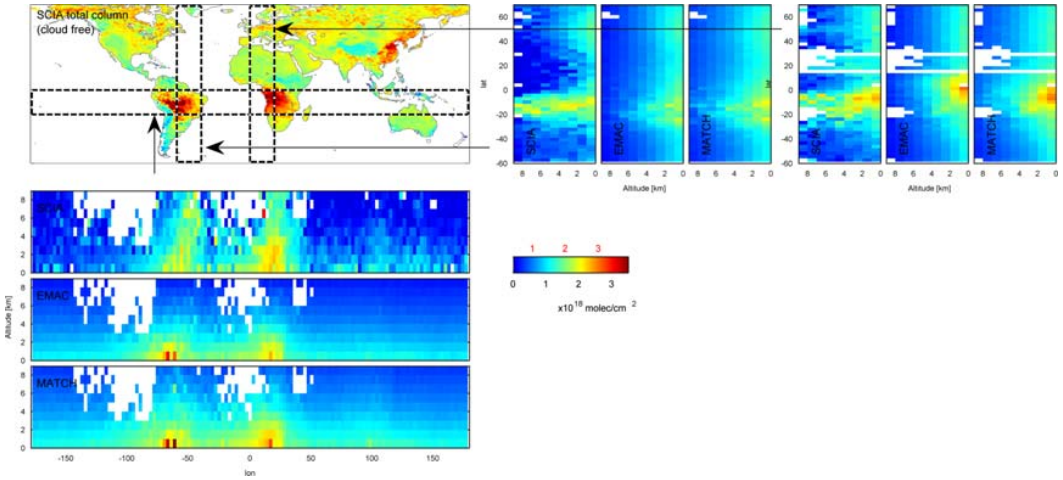

Fig. 7. Same as Fig. 5, but for July–September and for meridional and zonal cross sections over Africa and South America.

ACPD
13, 11659–11688, 2013

CO profiles from SCIAMACHY cloud slicing

C. Liu et al.